*Korean J. Chem. Eng.*, 37(11), 1951-1962 (2020)
DOI: 10.1007/s11814-020-0596-0

pISSN: 0256-1115
eISSN: 1975-7220

# Microwave-synthesized high-performance mesoporous SBA-15 silica materials for $CO_2$ capture

**Runa Dey and Arunkumar Samanta†**

Department of Chemical Engineering, Indian Institute of Technology (ISM), Dhanbad - 826004, Jharkhand, India
(*Received 8 November 2019 • Revised 14 May 2020 • Accepted 31 May 2020*)

**Abstract**−Microwave-assisted post-synthetic detemplating method was applied to remove successfully the occluded organic template from the mesoporous silica frameworks of as-synthesized SBA-15 within a short period of time compared to a conventional method, such as furnace calcination. The nitrogen adsorption/desorption isotherm studies showed that the resultant detemplated SBA-15 had a very high specific surface area of 1,271 $m^2$/g, large pore size of 9.21 nm and high pore volume of 2.10 $cm^3$/g; while the powder X-ray diffraction patterns and high-resolution TEM images of these support materials revealed the presence of highly ordered mesopores without any structural shrinkage. Both the microwave power and time during post-synthetic microwave irradiation were found to influence the morphological structure of the SBA-15 support. To evaluate the adsorption performance of the microwave-irradiated SBA-15 support, $CO_2$ adsorption uptake was measured after functionalizing it with different loadings of polyethyleneimine (PEI) under 9.7% $CO_2/N_2$ mixture at 75 °C. The maximum $CO_2$ uptake was 3.63 mmol $CO_2$/g (0.16 g/g), with an optimum PEI loading of 70 wt%. Because of the significant improvement in structural characteristics, the microwave-irradiated SBA-15 supports facilitated more PEI incorporation that contributed to about 15% higher $CO_2$ uptake than that of conventional furnace calcined one. In addition, the sorbent demonstrated very good cyclic stability when tested over 25 cycles and for a total duration of 20 h in humid conditions.

Keywords: SBA-15, Microwave, Detemplation, Calcination, Multicycle

## INTRODUCTION

The rising level of atmospheric carbon dioxide ($CO_2$), a major greenhouse gas, is attributed to gas emissions from coal-fired power plants and other anthropogenic sources that release biospheric carbon [1]. Thus, the development of improved and efficient technologies for fossil-fuel combustion and $CO_2$ capture for economic $CO_2$ sequestration is crucial.

The most potential retrofittable postcombustion $CO_2$ capture technology using aqueous alkanolamine-based absorption technique is still expensive and energy-intensive, mainly due to high energy requirement to regenerate the amine solvents, costs related to solvent loss, and corrosion of process equipment [2]. It is reported that aqueous amine-based $CO_2$ absorption is known to reduce the efficiency of a fossil-fuel based thermal power plant down by about 26% [3]. This has generated tremendous interest to exploring and developing a suitable, cost-effective alternative process technology for $CO_2$ capture and sequestration.

In recent years, among several technology options for postcombustion $CO_2$ capture, adsorption processes using amine-functionalized mesoporous siliceous solid supports, such as MCM-41 [4-7], MCM-48 [7], SBA-15 [8-10], MCF [11], KIT-6 [12] and other siliceous materials [13-16], have been promising alternatives to regenerative chemical absorption processes. Functionalized silica templated SBA-15 sorbents are among the most frequently studied mesoporous silica supports. SBA-15 supports have attracted much attention because of their large surface area, pore volume in comparison with other silica templated supports. Ahn and co-workers [17] compared the performance of different silica supports, such as MCM-41, SBA-15, and concluded that the pore diameter and pore arrangement of mesoporous silica materials reasonably influence the $CO_2$ sorption performance. Similar observations have also been reported [18,19]. Chen et al. [18] reported the outstanding performance of the PEI impregnated silica monolith that exhibited a multimodal hierarchical pore structure. It showed $CO_2$ adsorption capacity as high as 3.75 mmol $CO_2$/g under 5% $CO_2/N_2$ at 75 °C. This was attributed to the high pore volume of the monolith that can accommodate a larger amount of amine. Chen et al. [19] also found that the pore volume and pore size of the synthesized silica from power plant bottom ash was larger than conventionally synthesized SBA-15 and obtained equilibrium $CO_2$ adsorption capacity of 3.32 mmol $CO_2$/g with 60 wt% PEI. However, the effect of moisture on $CO_2$ adsorption capacity has not been investigated. Ma et al. [20] also reported that the $CO_2$ uptake capacity of PEI-functionalized SBA-15 sorbent was considerably higher than that of PEI-functionalized MCM-41 sorbent. This is because of more pore volume and larger pore diameter of SBA-15. Olea et al. [21] used pore expanded SBA-15 and reported a significant improvement in $CO_2$ adsorption capacity in comparison with their counterparts synthesized by a conventional method due to expanded pore channels.

Despite several advancements made during the past few years, there is still enough scope for improvement of the SBA-15 support quality to accommodate more functionalized active sites to enhance the $CO_2$ sorption capacity with fast adsorption/desorption kinetics

†To whom correspondence should be addressed.
E-mail: asamanta@iitism.ac.in

and long-term cyclic stability. For this reason, most of the recent research in the area of amine-functionalized SBA-15 sorbents has been oriented towards developing silica templated mesostructured framework addressing different aspects of synthesis. There are also considerable efforts to improve the synthesis methodologies that save time and energy without compromising the structural properties and simultaneously $CO_2$ adsorption performance. Regardless of differences in synthesis, final detemplating procedure that provides a stable framework with unclogged pore channels and higher silanol densities is an important step of each synthesis.

In conventional synthesis, to create the desired structural properties the structure-directing organic template that is occluded within the as-synthesized mesoporous framework is removed by extraction using conventional solvents or furnace calcination [22-24]. Tian et al. [25] reported that complete removal of the template from the silica framework is not possible using extraction. Lai et al. [26] studied the removal of the template from as-synthesized SBA-15 using solvent extraction method followed by microwave irradiation. However, they used a very large amount of ethanol/hexane (v/v, 1/1) solvent mixture (~0.2 L) for each gram of as-synthesized support to extract the surfactant template before microwaving. It suggests solvent extraction played the major role in the removal of the template. Therefore, for such microwave-assisted extraction, recovery of solvent could be a major drawback. On the other hand, furnace calcination, which is very easy in operation and is reported the most widely used technique for template removal, usually needs slow temperature ramps followed by an extended period of heating for about 6 h at nearly 550 °C and more energy. Moreover, it may also cause structural shrinkage [27]. Yuan et al. [28] applied plasma to remove template of SBA-15 and reported that more amines can be tethered due to high surface area and silanol density of SBA-15. However, the duration for plasma-assisted template removal was high. Therefore, more efforts are essential for developing a rapid method that can completely and effectively remove occluded template, preserving required morphological properties. Microwave-assisted template removal may alleviate such problems and offer a comparatively rapid and efficient method of preparing mesoporous materials. However, there is limited study on the synthesis of SBA-15 using microwave-assisted template removal, and to the best of our knowledge, there is no study to evaluate the performance of amine-functionalized SBA-15 synthesized by microwave-assisted detemplation method for postcombustion $CO_2$ capture.

In this study, microwave-assisted detemplation method was used for the removal of occluded organic template from as-synthesized SBA-15. The synthesized SBA-15 support and amine-functionalized sorbents were characterized using nitrogen adsorption/desorption isotherms, high resolution TEM (HRTEM), field emission SEM (FESEM), TGA and FTIR spectroscopy to assess the impact of microwave-assisted detemplating on their textural and morphological properties and $CO_2$ uptake performance. The adsorbents with optimum amine loading were tested for equilibrium $CO_2$ uptake, kinetics and multicycle stability using rapid temperature-swing adsorption/desorption methods. The experimental adsorption kinetic data were also correlated to the fractional-order kinetic model and goodness of the fit was assessed using average absolute deviation value.

## EXPERIMENTAL

### 1. Materials

The non-ionic copolymer, Pluronic P123 ($EO_{20}PO_{70}EO_{20}$, Average MW: ~5,800), tetraethylorthosilicate, TEOS (purity~98%), methanol (purity ~99%) and polyethyleneimine (PEI, Average MW: ~800) were purchased from Sigma-Aldrich and were used without further purification. Commercial mesoporous SBA-15 was purchased from Sigma Aldrich (CAS No. 7631-86-9). Aqueous hydrochloric acid solution (HCl) was purchased from Merck, India. Deionized water used was purified using a Milli-Q Integral 5 water purification system (Merck, USA). Carbon dioxide (purity~99.99%), $N_2$ (purity~99.999%) were purchased from Chemtron Science Laboratories Pvt. Ltd., India.

### 2. Preparation of As-synthesized SBA-15

The porous as-synthesized SBA-15 silica support was prepared according to the method reported by Zhao et al. [29] In a typical hydrothermal synthesis process, triblock copolymer, P123 was used as the template material, TEOS as the source of silica and HCl as a pH adjuster. Briefly, aqueous HCl (2 M) (120 cc) was mixed with P123 solution having Pluronic P123 (4 g) and deionized water (30 ml). The mixture was stirred vigorously at room temperature for about 2 h. After complete dissolution, the resultant mixture was transferred into a Teflon autoclave and maintained at ~40 °C. TEOS (8.5 g) was then added in drops into the solution under continuous stirring until a homogeneous mixture was obtained. After complete addition, the resultant gel was kept under slow stirring (100 rpm) at about 37±1 °C for 20 h. During this procedure, a milky white gel was formed in the Teflon autoclave. The content of the autoclave was then hydrothermally aged at 100 °C without stirring for about 48 h. The white precipitated product thus produced was filtered off through a Buchner funnel, and washed several times with a copious amount of deionized water. Finally, the produced as-synthesized SBA-15 mesostructured material was dried at room temperature and then in an air oven overnight at 80 °C.

### 3. Removal of Template

To remove the organic triblock copolymer template, P123 from as-synthesized SBA-15, post-synthesis detemplation method was carried out under rapid microwave irradiation in a 2.45 GHz microwave oven (LG MS2021CW, India), with adjustable power within the range of 70-700 W. In a typical process, as-synthesized SBA-15 samples weighing ~2 g were placed on a microwavable flat glass plate and then irradiated at desired microwave oven power (350, 500 and 700 W) for a particular duration. The samples were irradiated for 5 min, then the microwave power was turned off for approximately 2 min to cool the materials in the microwave oven cavity and turned back on again for 5 min to reheat the samples. This procedure was continued a few times until total irradiation time was reached. Care was taken to put the glass plate in the same place in the microwave oven for each treatment. The total irradiation time used was in the range of 20-60 min. The sample prepared in this way was designated as SMwP-T, where S refers to SBA-15, Mw refers to microwave irradiated, and P and T refers to microwave power (in Watt) and time duration (in min), respectively. For comparison, the template of as-synthesized SBA-15 was also removed in a muffle furnace (Thermcraft, USA) by conventional calcination in flowing air for 6 h at about 550 °C with a linear heating ramp of

2 °C/min. The resulting support sample obtained by this method was named as SFC, where S refers to SBA-15 and FC refers to furnace calcined.

**4. Functionalization of SBA-15**

To investigate the adsorption performance of the microwave irradiated SBA-15 support, amine functionalization was done using a branched polymeric amine, PEI. Functionalization of SMwP-T and SFC samples involved using the wet-impregnation method as described elsewhere [8] but with minor modifications. Initially, the desired amount of PEI and 10 ml of methanol was continuously sonicated for about 20 min to dissolve the PEI molecules and then approximately 2 g of previously dried, detemplated silica support was mixed in the solution. The resultant mixture was again ultrasonicated continuously in an ultrasonication bath (Elmasonic P, Germany) operated at 37 kHz with a power of 250 W for another 30 min at room temperature, to achieve uniform dispersion of the amine moieties inside the mesoporous support and then dried under high vacuum conditions at 80 °C for 2 h. These functionalized sorbents were denoted as SMwP-T/xPEI, and SFC/xPEI for microwave irradiated and furnace calcined SBA-15 supports, respectively. For comparison, commercial mesoporous SBA-15 (having a surface area of 750 $m^2$/g, pore size 5 nm, and pore volume 0.7 $cm^3$/g) was impregnated with PEI similar to the procedure mentioned above and was denoted as CSBA-15/xPEI, where x is the amine weight percent in the sorbent.

**5. Material Characterization**

Nitrogen adsorption/desorption isotherms of the detemplated SBA-15 support and PEI-functionalized sorbents were measured on a 3Flex surface characterization analyzer (Micromeritics, USA) at 77 K and in the relative pressure range, $P/P_0$ of 0-0.993. Initially, microwave irradiated support samples were outgassed overnight at 300 °C under high vacuum. However, amine-functionalized sorbents were outgassed at 80 °C for about 30 min to avoid amine loss. Multipoint Brunauer-Emmett-Teller (BET) method was used to measure the specific surface area ($S_{BET}$) at a relative pressure range of 0.05-0.30. The total pore volume ($v_p$) was calculated from the total adsorbed volume of liquid nitrogen at $P/P_0$ of 0.993. The distribution of pore size and average pore diameter ($d_{BJH}$) of samples were determined using the Barrett-Joyner-Halenda (BJH) method from the nitrogen desorption branch.

The surface morphology of the supports was examined using a FESEM (Supra 55, Carl Zeiss, Germany). The HRTEM micrographs of the calcined support samples were taken on a Technai $G^2$ S-Twin (FEI Netherlands) with 200 kV EFG source. A Cary 600 (Agilent, USA) equipped with a diamond attenuated total reflectance device was used to collect IR spectra of samples over the frequency range 4,000-400 $cm^{-1}$ and at a resolution of 2 $cm^{-1}$. Powder X-ray diffractograms (PXRD) of the materials were recorded on a BRUKER, Model-D8-ADVANCE diffractometer in the $2\theta$ range from 0.5° to 5.0° using the Cu K$\alpha$ monochromatic radiation with a wavelength of $\lambda$=0.1541 nm, 40 kV, 40 mA).

$CO_2$ adsorption isotherms of amine-functionalized sorbents were measured volumetrically with a Micromeritics 3Flex physisorption apparatus under a pressure range of 0-760 mm Hg. The adsorption isotherm experiments were conducted at various temperatures ranging from 20-75 °C maintained by a circulating water bath system. The bath temperature was maintained within ±0.1 °C of the required temperature level using a refrigerated circulator temperature controller (JULABO F25-ME, Germany). Prior to each adsorption measurement, the sorbents were outgassed at 80 °C for 30 min at constant vacuum to remove pre-adsorbed moisture and other gaseous impurities.

To study the $CO_2$ adsorption/desorption performance of the respective amine-functionalized SBA-15 sorbents, dynamic $CO_2$ uptake was also measured using a TGA (SDT Q600, TA Instruments Inc, USA). Before use, amine-functionalized sorbents were finely ground to mean particle size in the range of approximately 150-250 μm. For adsorption measurements, a gas mixture containing 9.7% $CO_2$ in $N_2$ (henceforth shortened to 9.7% $CO_2/N_2$) was used under atmospheric condition. In a typical procedure, approximately, 10-12 mg of the functionalized sorbents was loaded into a platinum crucible and preheated to 105 °C in a nitrogen stream (100 cc/min) for 60 min to eliminate adsorbed moisture and other impurities. The TGA temperature was then reduced to the desired sorption temperature, and the nitrogen gas was switched to premixed $CO_2/N_2$ gas mixture with a volumetric flow rate of 100 cc/min. The sorption temperature was maintained constant for 120 min.

Cyclic performance of the functionalized sorbents was also analyzed thermogravimetrically using 9.7% $CO_2/N_2$ gas mixture under dry and humid conditions at 75 °C for adsorption and pure nitrogen at 105 °C for regeneration. To study the $CO_2$ sorption capacity under humid condition, the 9.7% $CO_2/N_2$ dry gas mixture was passed through a saturator kept in a water bath maintained at 25 °C.

## RESULTS AND DISCUSSION

**1. Characterization of the Sorbent**

Nitrogen adsorption/desorption isotherms and pore size distribution of microwave irradiated and conventional muffle furnace calcined SBA-15 are shown in Fig. 1 and Fig. 2, respectively. All the isotherms of SBA-15 support materials were identified to be of

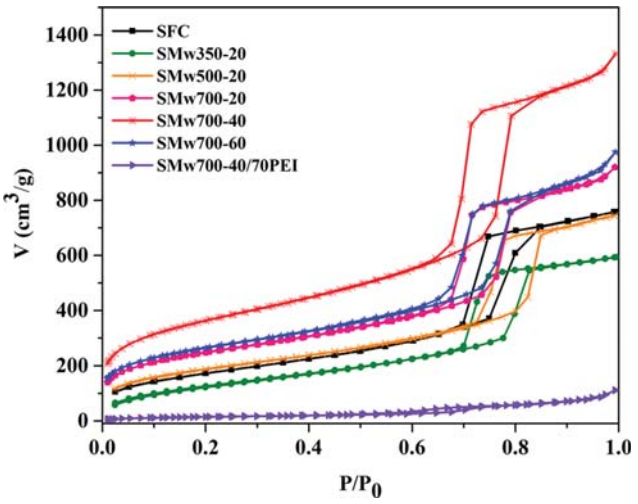


**Fig. 1. Nitrogen adsorption/desorption isotherms of SBA-15 and PEI-functionalized SBA-15 support at 77 K.**

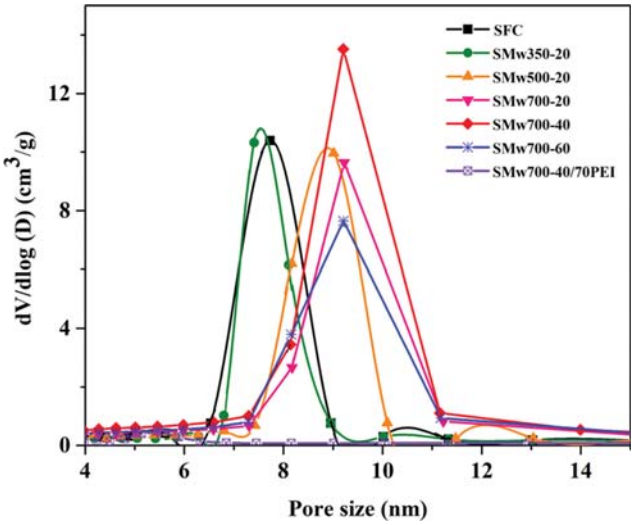


**Fig. 2. Pore size distribution of SBA-15 and PEI-functionalized SBA-15 support.**

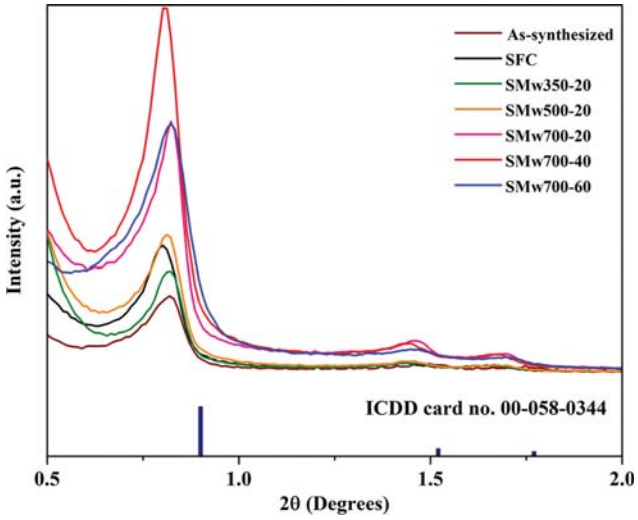


**Fig. 3. PXRD patterns of SBA-15 support.**

type IV physisorption isotherms. This confirmed the presence of typical mesopores in all the silica frameworks synthesized in this work. Furthermore, the existence of prominent hysteresis loops of $H_1$ type in all silica matrices indicated that SBA-15 supports have a relatively narrow distribution of uniform cylindrical pores [28]. The textural properties such as the BET surface area, BJH pore diameter, total pore volume estimated from nitrogen adsorption-desorption isotherms of various SBA-15 supports are given in Table 1. The highest specific surface area of 1,271 $m^2$/g and pore volume of 2.10 $cm^3$/g were obtained by microwave detemplation process. A comparison of these morphological data suggests interesting outcomes about the influence of microwave-assisted detemplating scheme on the mesoporous frameworks. Use of microwave detemplation of SBA-15 support leads to a significantly higher specific surface area, pore volume and BJH pore diameter than that obtained by conventional furnace calcination. However, amine impregnation greatly affected the nitrogen adsorption/desorption isotherms and BET surface area of SBA-15, which could be due to the pore blocking by the PEI amines.

The influence of microwave-assisted detemplation method in structural characterization of all SBA-15 samples is shown by the PXRD profiles in Fig. 3. All detemplated SBA-15 exhibited one sharp, intense diffraction peak (100) at $2\theta$ of approximately 0.79° and two relatively weak peaks for (110) and (200) planes at higher angles. This indicates the presence of well-ordered hexagonal pore arrays and 2-D pore structure in the silica supports. The PXRD measurements showed that SMw700-40 sorbent exhibited a shift towards the lower angle and narrow peak, which suggests there is no structural shrinkage; rather, the ordered structure of SBA-15 is successfully retained in the mesoporous matrix. The structural parameters such as unit cell parameter, $a_0$, and wall thickness, $w_d$, of microwave-assisted SBA-15 were also estimated using Eq. (1) and Eq. (2), respectively:

$$a_0 = \left(\frac{2}{\sqrt{3}}\right) d_{100} \quad (1)$$

$$w_d = a_0 - d_p \quad (2)$$

**Table 1. Structural parameters of SBA-15 support materials**

| SBA-15 sorbents | BET surface area ($m^2$/g) | Pore diameter (nm) | Pore volume ($cm^3$/g) | Interplanar spacing $d_{100}$ (nm) | Unit cell parameter $a_0$ (nm) | Wall thickness $w_d$ (nm) |
|---|---|---|---|---|---|---|
| CSBA-15 | 750[a] | 5.0[a] | 0.7[a] | - | - | - |
| SFC | 626±9[c] | 7.33±0.57[c] | 1.11±0.09[c] | 9.84 | 11.36 | 3.66 |
| SMw350-20 | 480[b] | 7.41[b] | 0.92[b] | 10.95 | 12.64 | 5.23 |
| SMw500-20 | 685[b] | 9.01[b] | 1.15[b] | 10.90 | 12.59 | 3.58 |
| SMw700-20 | 875±10[c] | 8.95±0.40[c] | 1.42±0[c] | 10.99 | 12.69 | 3.46 |
| SMw700-40 | 1262±13[c] | 9.23±0.02[c] | 2.05±0.07[c] | 11.17 | 12.90 | 3.69 |
| SMw700-60 | 936±19[c] | 9.22±0.01[c] | 1.52±0.03[c] | 10.91 | 12.59 | 3.38 |
| SMw700-40/70PEI | 54 | 5.47 | 0.20 | - | - | - |

[a]From product data sheet supplied by the manufacturer
[b]Only one valid measurement was obtained
[c]Standard deviation (SD) on duplicate measurements, where, SD is estimated from measurements of support material synthesized in different batches

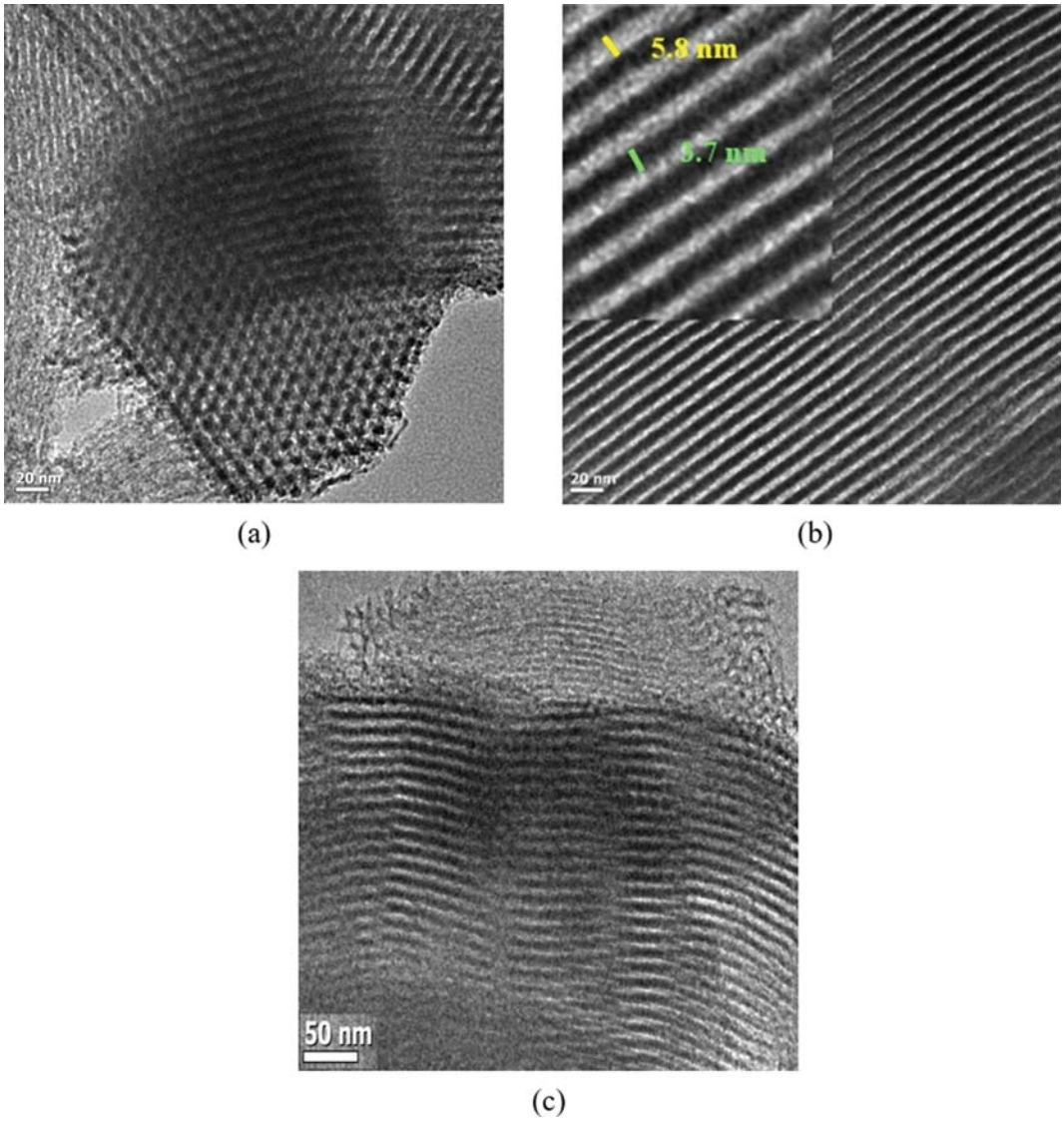


**Fig. 4. HRTEM images of (a) SMw700-40 (in perpendicular to the pore axis), (b) SMw700-40 and (c) SFC (in parallel to the pore axis).**

where, $d_p$ is the BJH pore diameter and $d_{100}$ is d-spacing of (100) diffraction peak estimated using Eq. (3):

$$d_{100} = \frac{1.5406}{2\sin\theta} \tag{3}$$

where, $\theta$ is the diffraction angle corresponding to (100) diffraction peak. The estimated structural parameters are listed in Table 1. As given in Table, SMw700-40 sorbents also exhibited the highest unit cell parameter value.

Fig. 4 depicts the HRTEM images obtained at perpendicular and at a parallel orientation to the pore direction. Fig. 4(a) shows HRTEM images obtained for the sample SMw700-40 as definitive evidence of the retention of a well-ordered hexagonal arrangement of 1-D mesopores. Additionally, the pore diameter and the wall thickness of the support were also measured from HRTEM and were found to be of 5.8 nm and 3.7 nm, respectively. These pore diameter values are in a close agreement with the values obtained from nitrogen adsorption/desorption isotherms and also corroborate the observations of PXRD profiles.

FESEM images of SMw700-40 and SFC support are also shown in Fig. 5. It can be seen that SBA-15 supports consist of wheat worm-like long rod-shaped morphologies. The length of the rods was found to be in the range of 0.7-1.9 μm and a thickness of 1-1.5 μm. After PEI impregnation, the sorbents still retained their original morphology and no variation in the morphology was detected (Fig. 5(c), and (d)).

A thermal analysis of each calcined SBA-15 support was also carried out in TGA to determine the template removal efficiency from the pore matrix of as-synthesized SBA-15 and are listed in Table 2. The thermal analysis of the sample was performed between room temperature to 650 °C at a heating rate of 10 °C/min under a pure nitrogen stream. The corresponding weight loss data are shown in Fig. 6. It clearly shows that the as-synthesized SBA-15 exhibits distinct weight loss behavior as compared to its calcined analogues due to the presence of greater amount of template. The final weight loss of As-synthesized, SFC, SMw350-20, SMw500-20, SMw700-20,

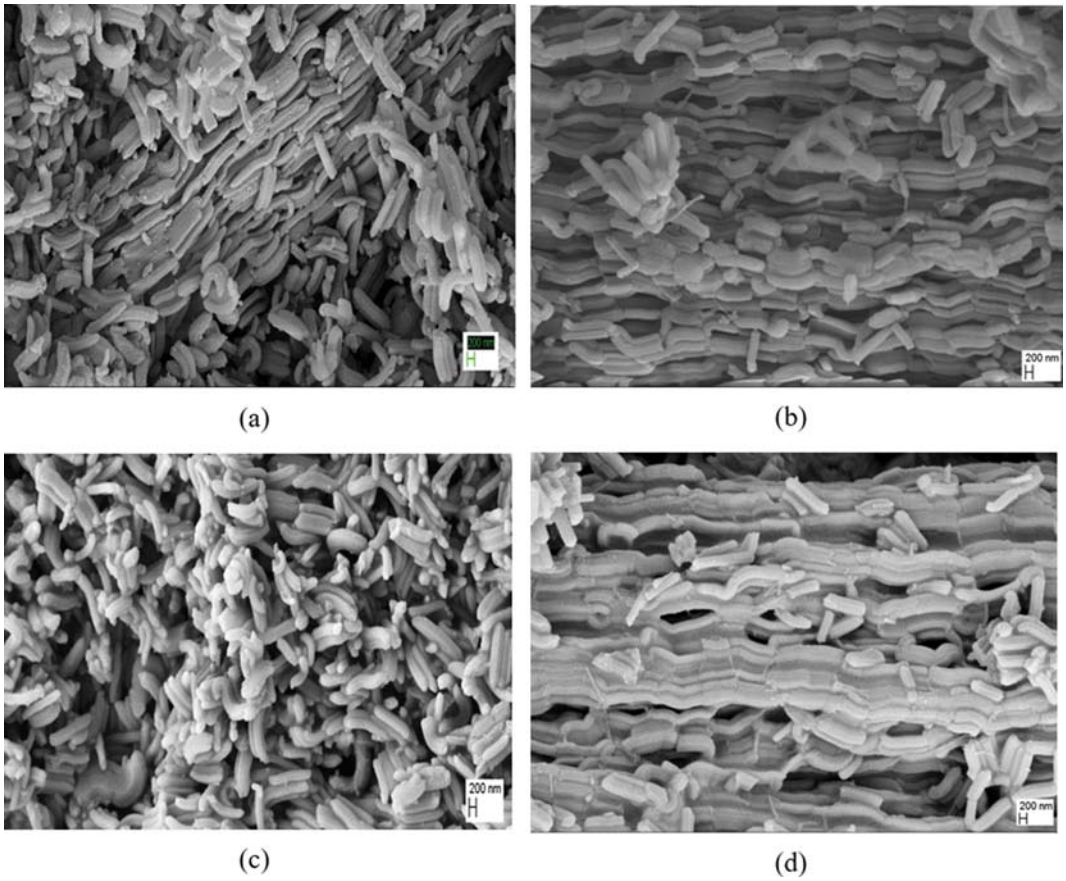


**Fig. 5. FESEM images of (a) SMw700-40 (b) SFC (c) SMw700-40/70PEI and (d) SFC/70PEI.**

**Table 2. Percentage removal of P123 template from SBA-15 support**

| SBA-15 support | % P123 removal* |
|---|---|
| SFC | 89.78 |
| SMw350-20 | 62.40 |
| SMw500-20 | 76.41 |
| SMw700-20 | 81.01 |
| SMw700-40 | 96.52 |
| SMw700-60 | 90.00 |

*% P123 removal $= \frac{(W_1 - W_2)}{W_1} \times 100$

where,

$W_1$=Wt% loss of P123 in as-synthesized SBA-15

$W_2$=Wt% loss of P123 in SBA-15 support

SMw700-40 and SMw700-60 samples (after deducting the moisture present) was 48.91%, 5.00%, 18.39%, 11.54%, 9.29%, 1.70% and 4.89%, respectively. Decreasing weight losses indicated successful detemplation process. The corresponding weight loss percentages are used to estimate the percentage removal of the template from SBA-15 matrix under various detemplation conditions. As can be seen from Table 2, microwave detemplation causes high percentage removal of P123. A nearly 96% removal of P123 can be obtained when SBA-15 is calcined at microwave conditions of 700 W, 40 min.

FTIR spectra of (a) as-synthesized, (b) furnace calcined and (c) microwave detemplated samples of SBA-15 supports were also recorded to ascertain the template removal from the mesoporous framework of SBA-15 silica and are shown in Fig. 7. The FTIR spectra have typical silica oxide patterns present in silica framework of SBA-15, including two intense peaks close to 801 and 1,070 $cm^{-1}$ which are assigned to symmetric and asymmetric Si-O-Si stretching vibrations, respectively, and a broad IR band in the

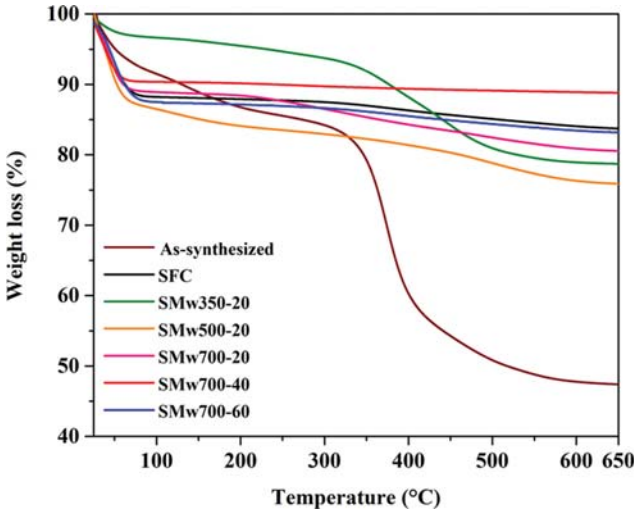


**Fig. 6. TGA profiles of SBA-15 support under nitrogen atmosphere.**

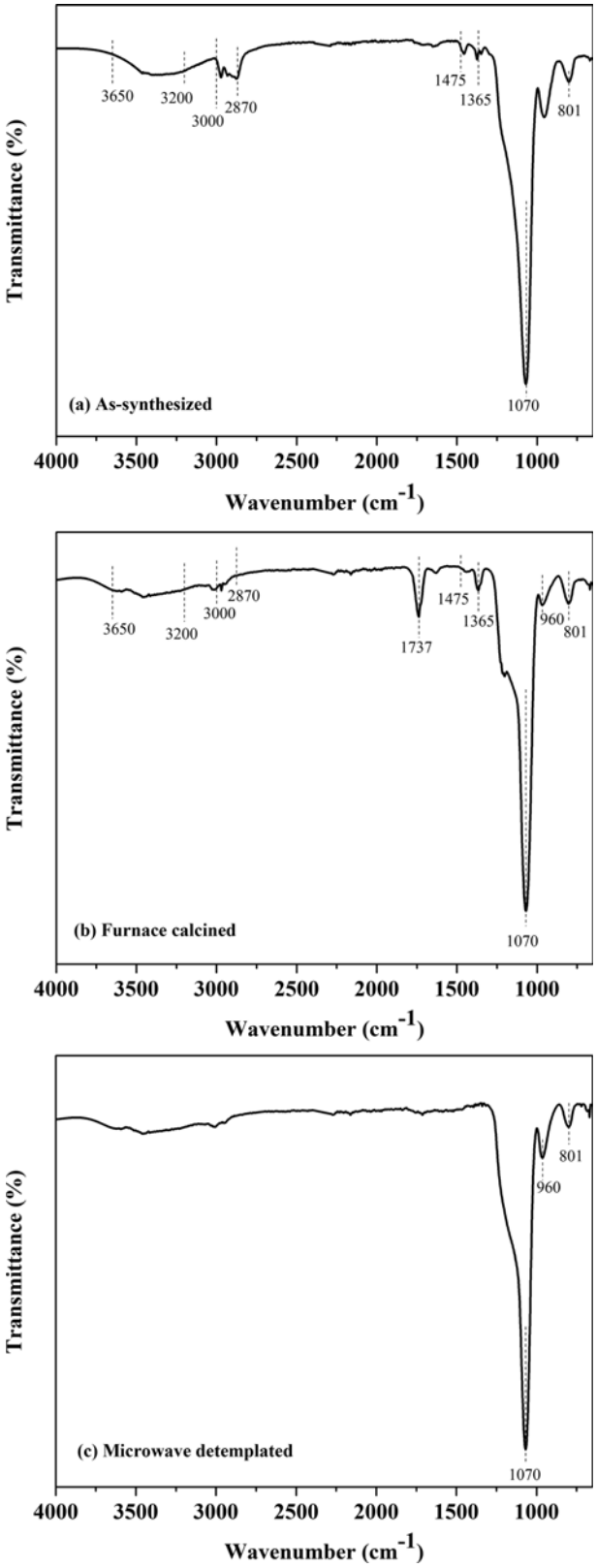


**Fig. 7. FTIR spectra (a) as-synthesized, (b) furnace calcined and (c) microwave detemplated SBA-15 support.**

hydroxyl region of 3,650-3,200 $cm^{-1}$ due to surface silanols and adsorbed moisture; a more detailed discussion on this is available elsewhere [8,9]. Therefore, in the context of detemplating procedure, some selected peaks of interest are identified for discussion. In particular, a group of transmittance peaks in the region of 3,000 to 2,870 $cm^{-1}$ and 1,475-1,365 $cm^{-1}$ as shown in Fig. 7(a) and (b). The former peaks in the region of 3,000 to 2,870 $cm^{-1}$ are associated due to the presence of C-H stretching and bending vibrations of $CH_2$ and $CH_3$ groups present in polyethylene oxide and polypropylene oxide blocks of the triblock copolymer template, P123, while a low intensity peak in the region 1,475-1,365 $cm^{-1}$ corresponds to the $CH_2$ and $CH_3$ bending peaks. These bands are distinctly visible in the as-synthesized SBA-15 sample and have slightly shifted and reduced in case of furnace calcined sample. This confirms the presence of the residuals of the template in the mesoporous frameworks of SBA-15. Whereas, all the peaks belonging to the organic template completely disappeared for microwave-assisted detemplated samples, which proves that the template was almost completely removed by microwave method. Another interesting observation is the presence of a distinct peak at about 1,737 $cm^{-1}$ (Fig. 7(b)), which corresponds to the stretching of carbonyl groups i.e. C=O groups, appearing on thermocalcined SBA-15 materials. This peak is not present in original organic copolymer template P123, and it appears only after calcination due to oxidation of P123 template. This indicates that the carbonaceous species formed during the thermocalcination step may have a carbonyl group, and this is completely avoided by detemplation process using microwave irradiation [30-32]. In addition, a relatively intense peak centered at ~960 $cm^{-1}$ was noticed for microwave detemplated SBA-15 (Fig. 7(c)) but much weaker for thermocalcined SBA-15. This peak is attributed to Si-OH bending vibration due to the presence of abundant silanol groups on the amorphous walls, especially on the surface of the mesoporous silica support and is well preserved after microwave calcination [28]. This also suggests furnace calcination relatively reduces silanol group density in compared to microwave-assisted detemplation process.

Thus, it can be seen that microwave power and time during microwave irradiation play a significant role in the removal of template and in the formation of porous network in SBA-15. For example, microwave irradiated supports with different microwave power and time showed PXRD profiles having the same diffraction peaks with intensities that gradually decreased as the microwave power and time increased. This decrease of intensity of diffraction peaks is mainly due to incomplete removal of template from mesoporous silica matrix. The more P123 is retained into the pore channels, the lower the peak intensity. However, there is minor shrinkage of peak intensity when microwave irradiation time was beyond 40 min for a microwave power of 700 W. This indicated a possible minor shrinkage of mesoporous structure due to higher irradiation time, i.e., the pore structure deformed in the presence of high energy flow 'thermal runaway' [33]. This observation can well be substantiated with multipoint BET specific surface area and total pore volume data obtained from nitrogen adsorption/desorption isotherms (shown in Fig. 1 and Table 1), and thermal analysis data obtained from TGA (shown in Table 2). From Table 1, it is clearly found that with further increase in microwaving time, keeping the power level constant, the surface area and pore volume decrease. The higher microwave power and more time are favorable to detem-

plate the as-synthesized SBA-15. Therefore, the microwave condition of 700 W, 40 min was selected as an optimum condition for detemplation.

All the above findings suggest that microwave detemplation method significantly enhances the morphological properties of silica supports as compared to conventional furnace calcination. These improved textural properties might be due to rapid uniform volumetric heating of whole material and microwave energy transfer phenomena [34,33]. In furnace calcination, heat is transferred to the surface of the material only by thermal conduction; while in microwave heating, microwave in the form of electromagnetic energy penetrates uniformly to the microstructure of the supports through molecular interactions with electromagnetic fields present and deposit energy. This probably causes a pumping action for the inner layer of molecules to force out to the surface, often as vapor, due to rapid rate of heating [35].

**2. $CO_2$ Adsorption Performance**

The introduction of different types of amine moieties such as PEI, TEPA etc. into the porous silica is of high interest with respect to the development of postcombustion $CO_2$ capture sorbents [8]. Since polymeric PEI molecules are reasonably more stable in the pore channels of silica support and exhibit relatively high $CO_2$ capture capacity, PEI was chosen here as model amine to study further the impact of amine loading on equilibrium $CO_2$ uptake using microwave-assisted SMw700-40 support. Based on the available pore volume data, (Table 1) and supposing that total pore volume is preferably occupied by PEI, it was estimated that the maximum possible PEI loadings could be about 70 wt%. As a result, to increase more amine into the support and, consequently, to achieve high $CO_2$ uptake, the selected synthesized sorbents were loaded with reasonably higher PEI loadings of 50-80 wt% and were studied for $CO_2$ adsorption capacity, kinetics and multicycle performance.

Initially, the actual amine loading of the sorbent was determined by TGA, and the results are depicted in Fig. 8 and also reported in Table 3. Thus, the theoretically estimated PEI loading, apparently showed no significant loss during PEI impregnation on SBA-15 supports. TGA and differential thermogravimetric (DTG) curves of each amine loaded sorbent exhibited three major steps of weight losses. At the beginning, a 1% weight loss at about 100 °C is mainly due to the desorption of physisorbed water vapor, while another

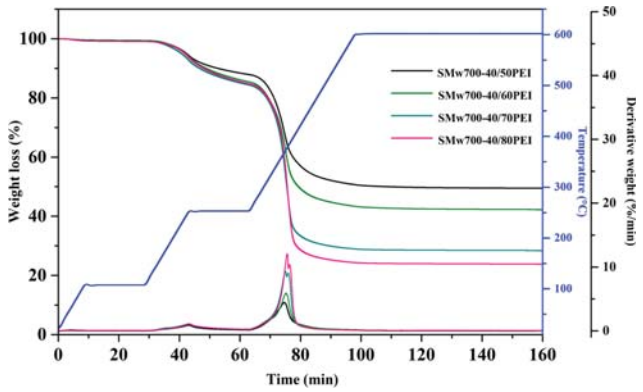


**Fig. 8. TGA and DTG profiles of PEI-functionalized SBA-15 sorbents.**

**Table 3. Estimated and actual PEI loading on SBA-15 sorbents**

| Wt% PEI (Estimated) | Wt% PEI (Actual) |
|---|---|
| 50 | 49.86 |
| 60 | 57.18 |
| 70 | 71.27 |
| 80 | 75.89 |

~14% weight loss occurring between 150 °C to 250 °C is due to the thermal disintegration of PEI which escaped from inner channels of the support framework during the temperature ramping. However, a significant decrease in weight loss observed above 350 °C is probably due to the possible self-condensation of part of free silanols and subsequent elimination of water molecules [36]. The DTG curves for all the sorbents with a sharp peak at around 370 °C represents the maximum mass loss event taking place. Thus, the results indicate that PEI modified SBA-15 sorbents are thermally stable at a temperature lower than 150 °C.

An earlier study [9] established that for PEI based chemisorption, optimal $CO_2$ adsorption temperature was 75 °C. Therefore, to investigate the impact of PEI loading on equilibrium $CO_2$ uptake, PEI-impregnated SMw700-40 sorbents containing 50-80 wt% PEI were evaluated under 9.7% $CO_2/N_2$ gas mixture at 75 °C. From Fig. 9, it is observed that $CO_2$ adsorption capacity increases with increase in the PEI content. However, at higher PEI beyond 70 °wt% there is a drop in $CO_2$ uptake. The sorbent attained the maximum equilibrium $CO_2$ uptake of 3.63 mmol $CO_2$/g (0.16 g $CO_2$ per g sample (hereafter shortened to g/g)) adsorbent with an amine efficiency of 0.223 at PEI loading of 70 wt%. This uptake capacity is about 15% higher than that obtained using SFC/70PEI. This enhanced $CO_2$ uptake can be explained in terms of improved and favorable textural properties of microwave detemplated SBA-15 support that helps in accommodating more PEI molecules that distribute uniformly within the support framework and create high $CO_2$ affinity sites to increase the probabilities of $CO_2$-amine interaction with-

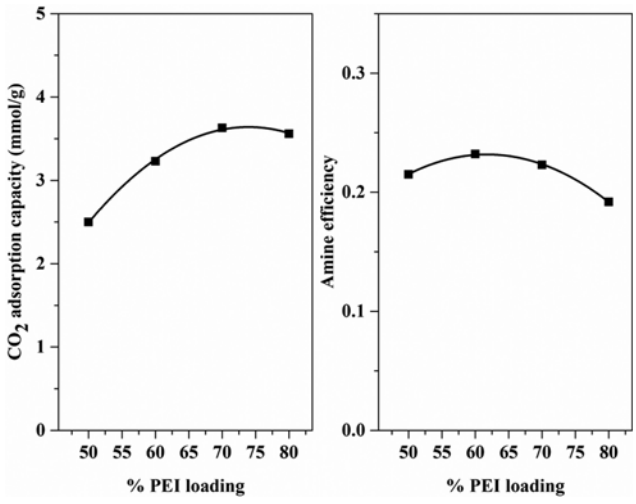


**Fig. 9. $CO_2$ uptake and amine efficiency of SMw700-40 with different PEI loadings.**

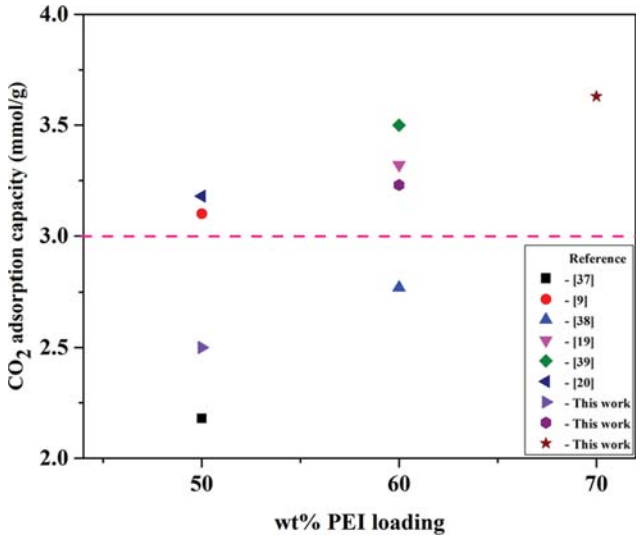


**Fig. 10. $CO_2$ adsorption capacity of various PEI-functionalized SBA-15 sorbents under 9.7% $CO_2/N_2$ and at 75 °C and 1 atm.**

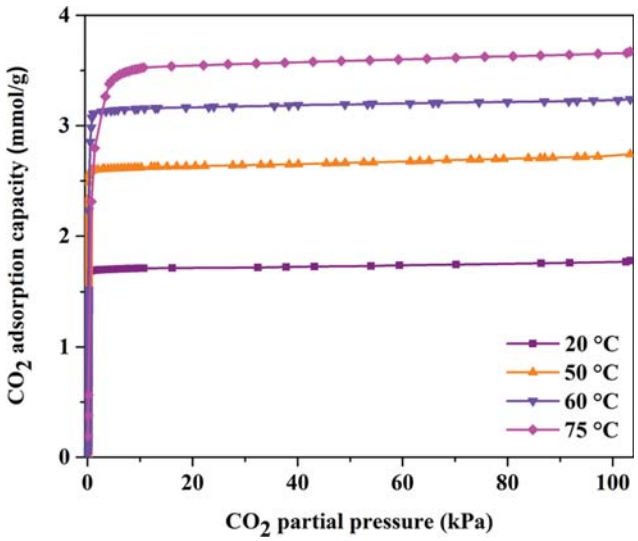


**Fig. 11. $CO_2$ adsorption isotherms of SMw700-40/70PEI at 20-75 °C.**

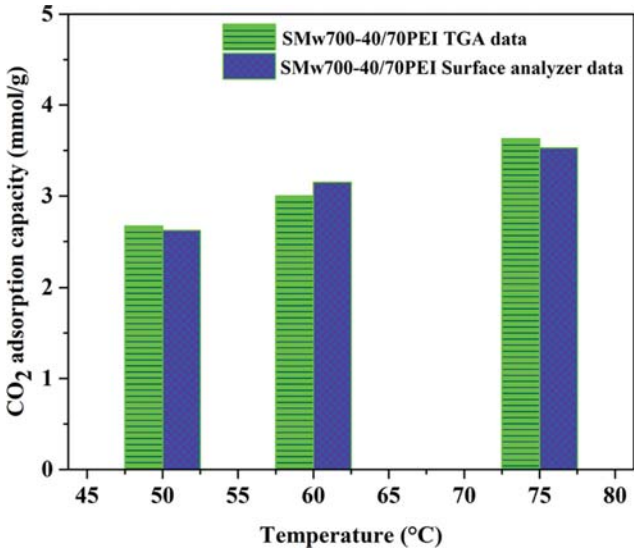


**Fig. 12. Comparison of equilibrium $CO_2$ adsorption capacity of SMw700-40/70PEI using volumetric and gravimetric $CO_2$ adsorption measurements.**

out deteriorating mass diffusivity during the adsorption process. As pointed out earlier, at higher PEI loadings beyond 70%, the excess PEI is probably accumulated on the external surface of the support that has partially clogged the silica pore channels, which in turn increases the diffusional resistance and thereby reduces $CO_2$-capturing affinity site and $CO_2$ uptake with low amine efficiency. The results also suggest optimal PEI loading is crucial in adsorption performance of PEI-impregnated silica supports.

Furthermore, a comparison of literature data available with respect to $CO_2$ uptake capacities of various PEI-functionalized SBA-15 is presented in Fig. 10. The sorbents considered here are mainly SBA-15/PEI which have $CO_2$ uptake capacity higher than the benchmark value of 2 mmol $CO_2$/g (0.088 g/g) at 75 °C under $CO_2/N_2$ gas mixture with a $CO_2$ concentration close to 10%. It clearly shows that the adsorption capacity achieved in this work using SMW700-40/70PEI sorbent is significantly higher than the benchmark $CO_2$ uptake capacity required. Besides, the $CO_2$ adsorption performance of CSBA-15/60PEI and CSBA-15/70PEI were also carried out under 9.7% $CO_2/N_2$ at a temperature of 75 °C and 1 atm. The comparison of the performance of CSBA-15 with that of their microwave irradiated one showed that the SMw700-40/70PEI outperformed CSBA-15/70PEI. Under similar adsorption conditions, SMw700-40/70PEI and CSBA-15/70PEI showed an adsorption capacity of 3.63 mmol/g (0.16 g/g) and 3.31 mmol/g (0.15 g/g), respectively.

Fig. 11 shows four $CO_2$ adsorption isotherms of SMw700-40/70PEI sorbent at a temperature range of 20-75 °C and pressures ranging up to 1 atm. It is observed that all the isotherms display a sharp rise of $CO_2$ adsorption capacity at very low-pressure region (below 10 kPa) followed by plateaus at a relatively higher pressures. The steep $CO_2$ adsorption isotherms indicate the strong interaction between sorbate $CO_2$ gas molecules and active PEI amine sites available on the silica support surface. The occurrence of plateau in isotherms between 10 to 100 kPa is due to the saturation of the sorbent particles and only physisorption of $CO_2$ on silica support is likely to be responsible. It shows the maximum amount of $CO_2$ uptake. These outcomes, therefore, also reveal that the equilibrium $CO_2$ capacity is relatively independent of $CO_2$ concentration in the bulk phase when $CO_2$ partial pressure is moderately high (above 10 kPa). Fig. 12 summarizes the equilibrium $CO_2$ adsorption capacity at P=100 kPa. Interestingly, as shown in Fig. 12, these results are consistent with the data obtained from gravimetric isotherm experiments using TGA carried out using $CO_2/N_2$ gas mixture with varying $CO_2$ partial pressures. Therefore, it is noteworthy that a high $CO_2$ uptake at reasonably low pressure resulting from chemical adsorption would negate energy-intensive pressurizing processes.

To comprehend the quality of the synthesized sorbent, it is of interest to understand the kinetics of adsorption of this new sorbent prepared by microwave irradiation method with its counterparts prepared using conventional furnace calcination technique.

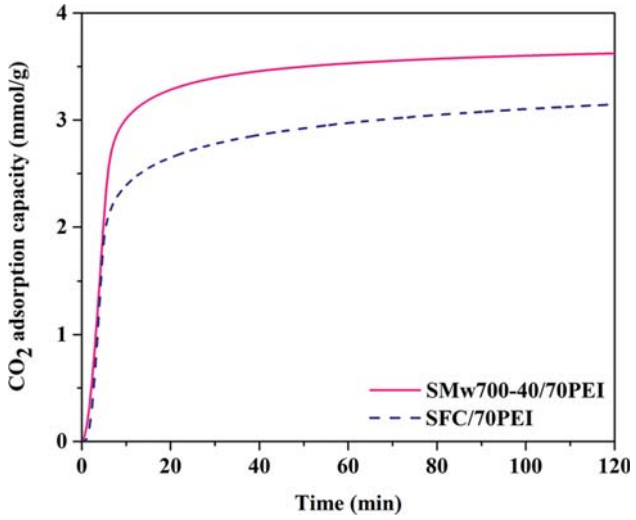


**Fig. 13. $CO_2$ uptake kinetics of PEI-impregnated SBA-15 sorbents at 75 °C under 9.7% $CO_2/N_2$.**

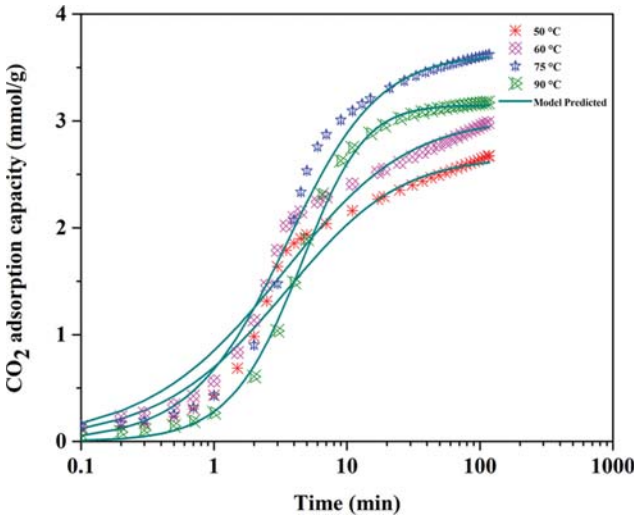


**Fig. 14. Experimental and model predicted $CO_2$ adsorption kinetics on SMw700-40/70PEI sorbent.**

Fig. 13 compares the kinetics of $CO_2$ adsorption between SMw700-40/70PEI and SFC/70PEI in 9.7%$CO_2/N_2$ at 75 °C and 1 atm. SMw700-40/70PEI exhibits a higher rate of adsorption as compared to SFC/70PEI and took only about 15 min to reach about 90% of the equilibrium adsorption capacity; while, for SFC/70PEI sorbent, it is about 30 min. The TGA weight gain curves show that at the beginning of adsorption, SMw700-40/70PEI and SFC/70PEI adsorbed $CO_2$ at the rate of 0.8750%/min and 0.5526%/min, respectively. This relatively high sorption rate might be due to the increase of total available pore volumes and enlargement of the average primary mesopore size of SMw700-40 material. All these influence in improving uniform dispersion of highly concentrated polymeric PEI suspension within the pores of the newly designed sorbent materials without increasing the diffusional resistance.

In addition, the fractional-order kinetic model (Eq. (4)), a general semi-empirical kinetic model proposed by Heydari-Gorji and Sayari [40] has been used to describe the measured dynamic $CO_2$ uptake data obtained at four different temperatures: 50, 60, 75 and 90 °C.

$$\frac{dq_t}{dt} = k_n t^{m-1}(q_e - q_t)^n \tag{4}$$

The integrated form of the Eq. (4) is given as

$$q_t = q_e - \left(q_e^{1-n} + \frac{n-1}{m} k_n t^m\right)^{\frac{1}{1-n}} \tag{5}$$

where, $q_t$ and $q_e$ are the instantaneous adsorption values at time t, and at equilibrium, respectively, and $k_n$, m and n are the model parameters. All these model parameters were estimated through a nonlinear least-square regression analysis using the Levenberg-Marquardt algorithm available in MATLAB optimization toolbox. The regression analysis was performed until the average absolute deviation (AAD) defined by Eq. (6) between the estimated and, experimentally obtained results was as low as possible.

$$\text{AAD}(\%) = \Sigma_{i=1}^{n} \frac{[(q_{t(exp)} - q_{t(mod)})/q_{t(exp)}]}{N-1} * 100 \tag{6}$$

where, $q_{t(exp)}$ is the experimentally observed adsorption capacity at a given time, $q_{t(mod)}$ is the estimated $CO_2$ uptake capacity and N is the number of data points.

The measured and estimated $CO_2$ uptakes from the correlation (Eq. (6)) for SMw700-40/70PEI sorbent are compared in Fig. 14. The estimated model parameters and kinetic constants with AAD values are presented in Table 4. The AAD values between the estimated and experimental $CO_2$ uptake data over the entire adsorption region and the temperatures studied are in the range of 1.42-2.47%. These significantly lower AAD values indicate that the $CO_2$ adsorption kinetics on SMw700-40/70PEI follows fractional-order kinetic model for all adsorption temperatures.

Multicycle stability with high $CO_2$ working capacity (defined for short adsorption time) is another important attribute to analyze the performance of an adsorbent and is useful in designing adsorption system for postcombustion $CO_2$ capture [41]. In a temperature-swing adsorption/desorption, 25 consecutive cycles were examined

**Table 4. Fitted parameter values using fractional-order kinetic model**

| Temp. (°C) | n | K | M | $q_e$ (mmol $CO_2$/g) | $q_{cal}$ (mmol $CO_2$/g) | AAD (%) |
|---|---|---|---|---|---|---|
| 50 | 1.6619 | 0.15 | 0.8548 | 2.6605 | 2.67 | 1.81 |
| 60 | 1.7047 | 0.1364 | 0.8001 | 3.0245 | 2.99 | 2.47 |
| 75 | 1.8368 | 0.0894 | 1.1662 | 3.6289 | 2.99 | 1.99 |
| 90 | 1.6447 | 0.0699 | 1.5255 | 3.1503 | 3.17 | 1.42 |

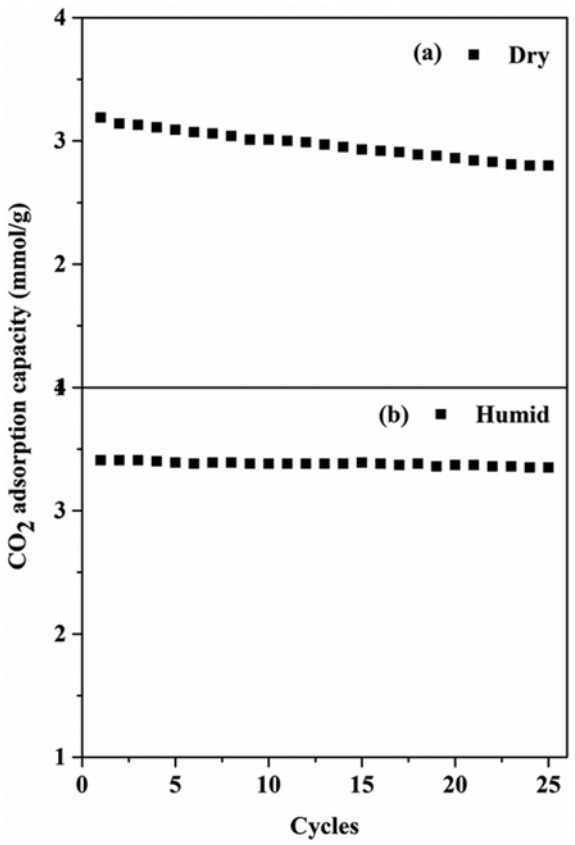


**Fig. 15. Cyclic adsorption/desorption of SMw700-40/70PEI sorbent under (a) dry and (b) humid conditions with $T_{adsorption}$= 75 °C for 30 min and $T_{desorption}$=105 °C for 20 min in 9.7% $CO_2/N_2$.**

using 9.7% $CO_2/N_2$ dry and humid gas mixtures, and are shown in Fig. 15. For each cycle, an adsorption temperature of 75 °C for 30 min and a regeneration temperature of 105 °C for 20 min were used. From Fig. 15, it is observed that the sorbent exhibited a $CO_2$ working capacity loss of about 12.2%, from 3.19 mmol $CO_2$/g (0.14 g/g) to 2.8 mmol $CO_2$/g (0.12 g/g) at the end of 25 cycles under dry $CO_2$ conditions. Using similar operating conditions but under humid condition, the working $CO_2$ capacity reduction was very less, only about 1.7%. This uptake loss under dry conditions could be due to (i) degradation of PEI, as it might form urea following the reaction pathway (Eq. (7)) [42] (ii) leaching or evaporation of low-molecular weight PEI chains.

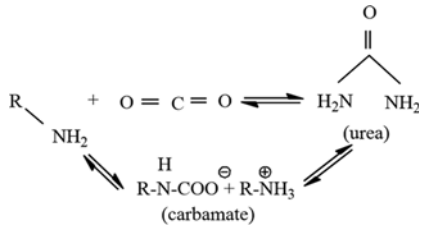


(7)

However, under humid conditions, the reaction mechanism with PEI is different. It follows a general base-catalyzed hydration of $CO_2$ (Eq. (8)) [40] and forms bicarbonate [43,44]. However, a marginal uptake loss is due to evaporative leaching of PEI monomers [8].

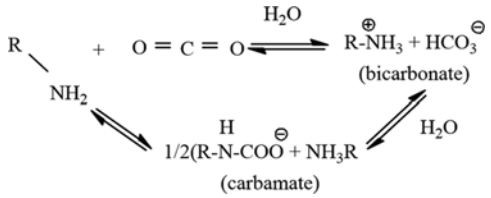


(8)

Therefore, these observations suggest that moisture present in flue gas has positive influence on $CO_2$ capture and, moreover, it has no adverse effects on the sorbent synthesized using microwave irradiated detemplation method.

## CONCLUSIONS

Microwave-assisted detemplating technique has been applied successfully for rapid removal of the organic surfactant template from as-synthesized mesoporous SBA-15. Without affecting the morphological characteristics of SBA-15 silica support, over 96% of detemplation from as-synthesized SBA-15 was achieved with 40 min of microwave irradiation using a microwave oven operating at 2.45 GHz with a power of 700 W. The percentage detemplation and consequently the textural properties such as surface area, pore volume and pore size of SBA-15 framework were found to largely depend on the microwave power and irradiation time. Compared with their conventional furnace calcined counterparts, the microwave-assisted detemplated SBA-15 silica materials have exhibited improved characteristics such as higher surface area (1,271 $m^2$/s), larger pore diameter (9.21 nm) with lower structural shrinkage. Because of these favourable structural attributes, microwaved SBA-15 silica sorbent accommodates more PEI moieties as high as 80 wt% within mesopores and consequently enhances $CO_2$ capture performance. The maximum $CO_2$ uptake achieved was 3.63 mmol $CO_2$/g (0.16 g/g) in 9.7% $CO_2/N_2$ at 75 °C. Various aspects of $CO_2$ sorption performance studies, such as the effect of PEI loading on $CO_2$ adsorption, $CO_2$ adsorption isotherms, kinetics of adsorption/desorption as well as multicycle stability studies, indicate that MwSBA/PEI is a promising sorbent for postcombustion $CO_2$ capture. In addition, a very good agreement between the experimental and model predicted dynamic $CO_2$ uptake with a maximum AAD of 2.47% shows that fractional-order kinetic model can successfully account for the $CO_2$ uptake dynamics on SMw700-40/70PEI in the temperature range of 50-90 °C under simulated gas having 9.7% $CO_2$. Eventually, this model is expected to support adsorber design for $CO_2$ removal using these solid sorbents.

Therefore, microwave irradiated detemplation method could be an alternative to conventional muffle furnace calcination to remove the occluded organic template with desired morphology.

## ACKNOWLEDGEMENTS

Runa Dey is thankful to Indian Institute of Technology (Indian School of Mines), Dhanbad, India for financial support in the form of a research scholarship.

## NOMENCLATURE

$a_0$ : unit cell parameter

$w_d$ : wall thickness
$d_p$ : BJH pore diameter
$d_{100}$ : d-spacing of (100) diffraction peak
$q_t$ : instantaneous adsorption values at time t
$q_e$ : instantaneous adsorption values at equilibrium
$k_n$, m and n : model parameters
AAD : average absolute deviation

**Greek Symbol**
$\theta$ : diffraction angle

## REFERENCES


1. U. Cubasch, D. Wuebbles, D. Chen, M. C. Facchini, D. Frame, N. Mahowald and J.-G. Winther, Introduction. In: Climate Change 2013: The Physical Science Basis. Contribution of Working Group I to the Fifth Assessment Report of the Intergovernmental Panel on Climate Change, T. F. Stocker, D. Qin, G.-K. Plattner, M. Tignor, S. K. Allen, J. Boschung, A. Nauels, Y. Xia, V. Bex and P. M. Midgley (eds.), Cambridge University Press, Cambridge, United Kingdom and New York, NY, USA (2013).
2. A. B. Rao and E. S. Rubin, *Environ. Sci. Technol.*, **36**, 4467 (2002).
3. D. Singh, E. Croiset, P. L. Douglas and M. A. Douglas, *Energy Convers. Manag.*, **44**, 3073 (2003).
4. M. Y. T. Le, S. Y. Lee and S. J. Park, *Int. J. Hydrogen Energy*, **39**, 12340 (2014).
5. Y. Choe, K.-J. Oh, S.-S. Kim and S.-W. Park, *Korean J. Chem. Eng.*, **27**, 962 (2010).
6. K.-S. Hwang, L. Han, D.-W. Park, K.-J. Oh, S.-S. Kim and S.-W. Park, *Korean J. Chem. Eng.*, **27**, 241 (2010).
7. P. Sharma, I.-H. Baek, Y.-W. Park, S.-C. Nam, J.-H. Park, S.-D. Park and S. Y. Park, *Korean J. Chem. Eng.*, **29**, 249 (2012).
8. A. Zhao, A. Samanta, P. Sarkar and R. Gupta, *Ind. Eng. Chem. Res.*, **52**, 6480 (2013).
9. R. Dey, R. Gupta and A. Samanta, *Sep. Sci. Technol.*, **53**, 2683 (2018).
10. E. S. Sanz-Pérez, M. Olivares-Marín, A. Arencibia, R. Sanz, G. Calleja and M. M. Maroto-Valer, *Int. J Greenh. Gas Con.*, **17**, 366 (2013).
11. Z. Liu, D. Pudasainee, Q. Liu and R. Gupta, *Sep. Purif. Technol.*, **156**, 259 (2015).
12. R. Kishor and A. K. Ghoshal, *Chem. Eng. J.*, **300**, 236 (2016).
13. T. Zhu, S. Yang, D. K. Choi and K. H. Row, *Korean J. Chem. Eng.*, **27**, 1910 (2010).
14. A. Boonpoke, S. Chiarakorn, N. Laosiripojana, S. Towprayoon and A. Chidthaisong, *Korean J. Chem. Eng.*, **29**, 89 (2012).
15. C. Chen, J. Kim and W. S. Ahn, *Korean J. Chem. Eng.*, **31**, 1919 (2014).
16. C. Manianglung, R. M. Pacia and Y. S. Ko, *Korean J. Chem. Eng.*, **36**, 1267 (2019).
17. W. J. Son, J. S. Choi and W. S. Ahn, *Micropor. Mesopor. Mater.*, **113**, 31 (2008).
18. C. Chen, S. T. Yang, W. S. Ahn and R. Ryoo, *Chem. Commun.*, **24**, 3627 (2009).
19. C. Chen, K. S. You, J. W. Ahn and W. S. Ahn, *Korean J. Chem. Eng.*, **27**, 1010 (2010).
20. X. Ma, X. Wang and C. Song, *J. Am. Chem. Soc.*, **131**, 5777 (2009).
21. A. Olea, E. S. Sanz-Perez, A. Arencibia, R. Sanz and G. Calleja, *Adsorption*, **19**, 2 (2013).
22. Y. K. Bae and O. H. Han, *Micropor. Mesopor. Mater.*, **106**, 304 (2007).
23. L. C. C. Silva, T. V. S. Reis, I. C. Cosentino, M. C. A. Fantini, J. R. Matos and R. E. Bruns, *Micropor. Mesopor. Mater.*, **133**, 1 (2010).
24. F. Kleitz, W. Schmidt and F. Schuth, *Micropor. Mesopor. Mater.*, **65**, 1 (2003).
25. B. Tian, X. Liu, C. Yu, F. Gao, Q. Luo, S. Xie, B. Tu and D. Zhao, *Chem. Commun.*, **11**, 1186 (2002).
26. T. L. Lai, Y. Y. Shu, Y. C. Lin, W. N. Chen and C. B. Wang, *Mater. Lett.*, **63**, 1693 (2009).
27. S. G. d. Avila, L. C. C. Silva and J. R. Matos, *Micropor. Mesopor. Mater.*, **234**, 277 (2016).
28. M. H. Yuan, L. Wang and R. T. Yang, *Langmuir*, **30**, 8124 (2014).
29. D. Zhao, J. Feng, Q. Huo, N. Melosh, G. H. Fredrickson, B. F. Chmelka and G. D. Stucky, *Science*, **279**, 548 (1998).
30. F. Berube and S. Kaliaguine, *Micropor. Mesopor. Mater.*, **115**, 469 (2008).
31. M. Barczak, K. Michalak-Zwierz, K. Gdula, K. Tyszczuk-Rotko, R. Dobrowolski and A. Dabrowski, *Micropor. Mesopor. Mater.*, **211**, 162 (2015).
32. M. S. Yilmaz and S. Piskin, *J. Therm. Anal. Calorim.*, **121**, 1255 (2015).
33. Z. Peng and J.-Y. Hwang, *Int. Mater. Rev.*, **60**, 30 (2015).
34. L. F. Chen, C. K. Ong, C. P. Neo, V. V. Varadan and V. K. Varadan, *Microwave electronics: Measurement and materials characterization*, John Wiley & Sons. Ltd., USA (2004).
35. A. S. Mujumdar, *Handbook of industrial drying*, fourth Ed., CRC, Boca Raton (2006).
36. X. Xu, C. Song, J. M. Andresen, B. G. Miller and A. W. Scaroni, *Energy Fuels*, **16**, 1463 (2002).
37. J. Liu, D. Cheng, Y. Liu and Z. Wu, *Energy Fuels*, **27**, 5416 (2013).
38. W. Klinthong, C. H. Huang and C. S. Tan, *Ind. Eng. Chem. Res.*, **55**, 6481 (2016).
39. X. Wang, X. Ma, C. Song, D. R. Locke, S. Siefert, R. E. Winans, J. Möllmer, M. Lange, A. Möller and R. Gläser, *Micropor. Mesopor. Mater.*, **169**, 103 (2013).
40. A. Heydari-Gorji and A. Sayari, *Chem. Eng. J.*, **173**, 72 (2011).
41. A. Samanta, A. Zhao, G. K. H. Shimizu, P. Sarkar and R. Gupta, *Ind. Eng. Chem. Res.*, **51**, 1438 (2012).
42. A. Sayari and Y. Belmabkhout, *J. Am. Chem. Soc.*, **132**, 6312 (2010).
43. G. Sartori and D. W. Savage, *Ind. Eng. Chem. Fundam.*, **22**, 239 (1983).
44. T. L. Donaldson, Y. N. Nguyen, *Ind. Eng. Chem. Fundam.*, **19**, 260 (1980).